Atmospheric Environment 105 (2015) 202–211

Contents lists available at ScienceDirect

Atmospheric Environment

journal homepage: www.elsevier.com/locate/atmosenv

Numerical simulation of the interaction between ammonium nitrate aerosol and convective boundary-layer dynamics

E. Barbaro [a, *], M.C. Krol [a, b], J. Vilà-Guerau de Arellano [a]

[a] Meteorology and Air Quality Section, Wageningen University, The Netherlands
[b] Institute for Marine and Atmospheric Research Utrecht, Utrecht University, The Netherlands

HIGHLIGHTS

- Using a LES model we find a strong interaction between 3D-turbulence and $^{A}NO_3$.
- The apparent deposition of $^{A}NO_3$ is larger for shorter equilibration timescales.
- The transport of $^{A}NO_3$ in 1D models needs a larger exchange coefficient than heat.

ARTICLE INFO

Article history:
Received 16 September 2014
Received in revised form
15 January 2015
Accepted 21 January 2015
Available online 24 January 2015

Keywords:
Gas-aerosol conversion
Convective boundary-layer dynamics
Aerosol nitrate deposition
Reactive turbulent exchange coefficient
Large-Eddy simulation

ABSTRACT

We investigate the interaction between the ammonium nitrate aerosol ($^{A}NO_3$) abundance and convective boundary-layer (CBL) dynamics by means of a large-eddy simulation (LES) framework. In our LES model the CBL dynamics is solved coupled with radiation, chemistry, and surface exchange. Concerning the aerosol coupling we assume a simplified representation that accounts for black carbon, aerosol water and inorganic aerosols, focusing on the semi-volatile ammonium nitrate aerosol within the CBL. The aerosol absorption and scattering of shortwave radiation is also taken into consideration. We use a data set of observations taken at the Cabauw Experimental Site for Atmospheric Research during the IMPACT/EUCAARI (European Integrated Project on Aerosol, Cloud, Climate, and Air Quality Interactions) campaign to successfully evaluate our LES approach. We highlight that our LES framework reproduces the observations of the ratio between gas-phase nitrate and total nitrate at the surface, with a diurnally-averaged overestimation of only $\approx$12%. We show that the dependence between gas-aerosol conversion of nitrate and CBL (thermo)dynamics produces highly non-linear concentration and turbulent flux vertical profiles. The flux profiles maximize at around 1/3 of the CBL. Close to the surface, we show that the outgassing of $^{A}NO_3$ affects the dry deposition of nitrate. This outgassing is responsible for the high deposition velocities obtained from the concentration and flux measurements during observational campaigns. To account for the influence of CBL (thermo)dynamics on gas-aerosol conversion we propose an effective turbulent exchange coefficient based on an analysis of the flux budget equation of aerosol nitrate calculated by our LES. The implementation of this effective turbulent exchange coefficient in a 1D model leads to a better agreement with the LES results and with surface observations.

1. Introduction

The role of tropospheric aerosols in the climate system has been exhaustively studied over the past decades (Jacobson, 1998; Kaufman et al., 2002; Bellouin et al., 2005). According to a recent overview of Baklanov et al. (2014), however, the online coupling of atmospheric dynamics, aerosol transport, chemical reactions, and atmospheric composition in numerical models will remain a challenge over the next years. Specifically for the convective boundary layer (CBL) only in the last decade a few integrating studies appeared that couple aerosols to boundary-layer dynamics, microphysics and chemistry (Jiang and Feingold, 2006; Barbaro et al., 2014; Lee et al., 2014). The same is noted from the observational perspective. Several measurement campaigns have established a comprehensive database of meteorological observations (Angevine et al., 1998; Masson et al., 2008) often including

* Corresponding author.
E-mail address: eduardo.wildebarbaro@wur.nl (E. Barbaro).

http://dx.doi.org/10.1016/j.atmosenv.2015.01.048
1352-2310/

radiosondes of the CBL vertical structure. However, only a few have combined these with detailed aerosol and chemical observations (Kulmala et al., 2011; Jager, 2014).

In this paper we study the formation and transport of ammonium nitrate aerosol (henceforth called $^{A}NO_3$) within the CBL placing special emphasis on understanding and representing processes such as the deposition flux and turbulent transport. Extending previous studies (Vinuesa and Vilà-Guerau de Arellano, 2003; Vilà-Guerau de Arellano et al., 2005; Aan de Brugh et al., 2013; Barbaro et al., 2014) we present here a Large-Eddy Simulation (LES) modeling framework. The novelty of this study lies in the dynamical coupling of the CBL (thermo)dynamics and turbulence with the surface, radiation, chemistry, and aerosols. At the surface, we explicitly solve the energy budget and account for bi-directional turbulent flux exchanges of chemical species.

Aan de Brugh et al. (2013) have shown by means of an LES (albeit without accounting for deposition effects and chemistry) that fast vertical mixing in the CBL in combination with a temperature-dependent partitioning of atmospheric nitrate between the gas and aerosol phases lead to interactions between dynamics and aerosol formation. Close to the top of the CBL (cooler) gaseous nitric acid (henceforth called $^{g}HNO_3$) and ammonia (NH_3) condense on $^{A}NO_3$, thus the gas-aerosol equilibrium shifts towards the aerosol phase. Close to the surface (warmer) $^{A}NO_3$ evaporates to $^{g}HNO_3$ shifting the equilibrium towards the gas-phase.

The outgassing of $^{A}NO_3$ close to the surface significantly affects the dry deposition of nitrate since its deposition velocity depends upon whether nitrate is in the gas or particle phase (Huebert and Robert, 1985; Mozurkewich, 1993; Nemitz and Sutton, 2004). This has implications especially for the measurement community since the gas-aerosol equilibrium may change below the measurements height (Huebert et al., 1988; Wolff et al., 2010). As a result, several studies report very high aerosol nitrate deposition velocities (Hanson, 1991) since the actual measurements reflect a so-called "apparent deposition" (Nemitz and Sutton, 2004).

According to previous studies (Harrison and Pio, 1983; Mozurkewich, 1993; Nemitz and Sutton, 2004; Morino et al., 2006; Fountoukis and Nenes, 2007; Aan de Brugh et al., 2013) the physical mechanisms that drive the gas-aerosol nitrate spatial distribution are: (i) the availability of NH_3 and SO_4^{2-}, (ii) CBL (thermo)dynamics, (iii) gas-aerosol equilibration timescale (τ_{eq}), and (iv) dry deposition of gas phase nitrate. As discussed in previous work (Morino et al., 2006; Fountoukis and Nenes, 2007; Aan de Brugh et al., 2012), τ_{eq} is the effective timescale required for ammonia and gaseous nitric acid to reach equilibrium with the inorganic aerosol particles. Several studies estimated that τ_{eq} for aerosol nitrate ranges from a few seconds to several minutes, i.e. τ_{eq} is of similar order of magnitude as the turbulent timescale of the CBL (Dassios and Pandis, 1999; Morino et al., 2006; Aan de Brugh et al., 2013). In such circumstances, non-linearities between CBL dynamics and chemistry are expected (Fitzjarrald and Lenschow, 1983; Krol et al., 2000; Vinuesa and Vilà-Guerau de Arellano, 2003). Despite its importance, an accurate representation of τ_{eq} from the observational point of view remains challenging, since τ_{eq} depends on microphysical properties of aerosols, e.g. viscosity and particle size (Shiraiwa and Seinfeld, 2012; Saleh et al., 2013), and CBL (thermo)dynamics (Morino et al., 2006).

Most atmospheric models use standard diffusion theory (K-theory) to parametrize the vertical turbulent flux of chemical species (Hamba, 1993; Vilà-Guerau de Arellano and Duynkerke, 1995; Hesterberg et al., 1996; Nemitz et al., 2004; Aan de Brugh et al., 2012). In this approach the exchange coefficient for heat or moisture is also used for chemical species. For inert scalars or long-lived species, standard diffusion theory has been proven sufficiently accurate to represent the turbulent vertical transport (Vilà-Guerau de Arellano and Duynkerke, 1995). For short-lived species, it has been suggested to adapt the exchange coefficient taking the chemical timescale into account (Vilà-Guerau de Arellano and Duynkerke, 1992).

In this paper, we revisit the gas-aerosol partitioning of nitrate in the CBL using our coupled LES framework. We focus on two outstanding issues concerning nitrate. First, we will investigate the impact of CBL turbulence and chemistry on nitrate deposition. LES results will be used to calculate the nitrate deposition velocity for two values of τ_{eq}. Second, we investigate the question how to parametrize turbulent vertical flux accounting for the interaction between turbulence and the gas-aerosol conversion of nitrate (both explicitly solved in our LES) in non-eddy-resolving models. Consequently, we will derive a parametrization for transport of gas and aerosol nitrate and apply it in the Wageningen University Single Column model (WUSCM).

2. Methods

2.1. Numerical modeling framework

We investigate the evolution of the ammonium nitrate concentration within the CBL by means of an LES framework. The use of LES allows us to solve explicitly the most energetic turbulent eddies and parametrize only the smallest scales (see supplementary material, from now on SM). We use the Dutch Atmospheric LES (DALES, version 3.2 – see Heus et al. (2010) for details). We implemented ISORROPIA2 (Nenes et al., 1998; Fountoukis and Nenes, 2007) to interactively account for the equilibrium between gas-phase and aerosol nitrate. The aerosol properties (extinction, single scattering albedo – ω, and asymmetry factor – g) are dynamically calculated in DALES by means of an aerosol module, as explained in detail in Aan de Brugh et al. (2012). The aerosols are also coupled to the shortwave (SW) radiation calculations by means of the broadband two-stream Delta–Eddington model, as discussed in Barbaro et al. (2014). We parametrize dry deposition of gas-phase chemicals and aerosols similarly to Ganzeveld and Lelieveld (1995) and Slinn and Slinn (1980) respectively, and the surface energy budget equations are calculated based on van Heerwaarden et al. (2010). A detailed description of the SW radiation and land-surface modules, and their coupling in DALES, was already given by Barbaro et al. (2014). Therefore, we here focus on a description of the chemistry, aerosol, and dry deposition modules.

2.1.1. Chemistry module

The simple background gas-phase chemical utilized here was already used in several DALES studies (Vilà-Guerau de Arellano et al., 2011) and we will show that realistic distributions of the main chemicals species are simulated. Our main goal is to ensure a satisfactory reproduction of the NO–NO_2-O_3 triad and an accurate formation rate of $^{g}HNO_3$ from the oxidation of NO_2 ($OH + NO_2 \rightarrow {}^{g}HNO_3$).

In the SM we provide the 3D conservation equation for the resolved scalar spatial and temporal distributions in DALES. Here, as a process illustration of the coupling between dynamics and the chemistry, we show in Eq. (1) the 1D conservation equation of the aerosol nitrate for a horizontally averaged CBL explicitly including the gas-particle conversion:

$$\frac{\partial^{A}\overline{NO_3}}{\partial t} = -\frac{\partial \overline{w'^{A}NO_3'}}{\partial z} + \frac{\overline{^{A}NO_3^{eq}} - \overline{^{A}NO_3}}{\tau_{eq}}, \quad (1)$$

where the first term on the right hand side is the vertical turbulent flux divergence of nitrate explicitly solved by our LES (but

parameterized in 1D models), and the last term represents the temperature dependent gas-particle conversion. Similarly to Nemitz and Sutton (2004), we write the gas-particle conversion term as the difference between the $^{A}NO_3$ equilibrium ($^{A}NO_3^{eq}$) calculated by ISORROPIA2 and the actual $^{A}NO_3$ concentration divided by τ_{eq} for nitrate. The dependence of the gas-aerosol nitrate equilibrium on absolute temperature and relative humidity is carefully discussed in Mozurkewich (1993) and Nenes et al. (1998). The equilibrium is obtained provided the total concentrations of nitrate and ammonia, (TNO_3 and TNH_4, respectively) absolute temperature and relative humidity (Mozurkewich, 1993; Aan de Brugh et al., 2013). These fields are dynamically obtained from the LES and serve as input parameters for the ISORROPIA2 calculations.

2.1.2. Aerosol module

The optical properties of inorganic and black carbon (BC) aerosols are calculated assuming two log-normal aerosol size distributions ($\bar{r} = 75$ nm and 37 nm, respectively and $\sigma = 2$, where r is the radius and σ the standard deviation of both the distributions). The first mode represents an accumulation soluble aerosol and the second mode an insoluble aerosol (containing only black carbon). Analogous to Aan de Brugh et al. (2012), we assume all the inorganic aerosols to be spherical and contain only water, ammonium nitrate and ammonium sulfate. The insoluble BC particles are assumed to be externally mixed with the soluble particles. Similarly to Aan de Brugh et al. (2012) our model does not take into account organic aerosol. The lack of organic aerosols can cause an underestimation of the extinction coefficient since it represents a significant component of particulate matter in the Netherlands (Dusek et al., 2013). Since ultimately our intent is to reproduce the correct effect of the aerosols on the surface net-radiation (Barbaro et al., 2014) we compensate the absence of organic aerosols by introducing aerosol nitrate, aerosol sulfate and black carbon in the free atmosphere according to the observations of aerosol optical depth (τ) and single scattering albedo as we detail in Sect. 3.

2.1.3. Dry-deposition module

The dry-deposition velocities for gaseous species (v_d) are parametrized as described in Ganzeveld and Lelieveld (1995). Similarly, we take $v_d = (r_a + r_b + r_c)^{-1}$ where r_a is the aerodynamic resistance between the first level of the LES model (15 m in our case) and the surface, r_b is the quasi laminar sublayer resistance (depending on the gas and its molecular diffusivity) and r_c the bulk surface resistance. The dry-deposition for aerosols is calculated as $v_d^a = (r_a + r_d)^{-1}$ and is based on Slinn and Slinn (1980). In their approach v_d^a is related directly to the resistance terms, where r_d accounts for the contributions of Brownian diffusion and impaction. Our aerosols are sub-micron particles, and the gravitational term can be safely neglected. We perform our simulations over a typical grassland (90% vegetated) with a constant surface roughness of 15 cm. The dry-deposition model implemented in our framework is similar to the scheme implemented in the TM5 chemical transport model (Krol et al., 2005) and has been widely used in several studies (Huijnen et al., 2010).

2.2. Observational data set

We design our LES experiments based on observations taken on May 8, 2008 at CESAR (Cabauw Experimental Site for Atmospheric Research – www.cesar-observatory.nl), in the Netherlands during the IMPACT/EUCAARI intensive measurement campaign (Kulmala et al., 2011). We choose May 8, 2008 (hereafter CESAR2008) due to the availability of observations and the appropriate synoptic situation, characterized by a persistent high pressure system above central Europe favoring clear-sky conditions during the entire day (Hamburger et al., 2011). The observations were extensively validated by Wang et al. (2009) (direct/diffuse SW radiation), Hamburger et al. (2011) (synoptics and pollution), Aan de Brugh et al. (2012) (gas-aerosol conversion) and Barbaro et al. (2014) (thermodynamics, CBL height and energy/radiation budgets). The hourly integrated gas-phase and aerosol nitrate, as well as the ammonia observations used in this work were measured simultaneously by a MARGA (Monitor for AeRosols and Gases in ambient Air) system as described in Aan de Brugh et al. (2012) and Mensah et al. (2012). In a MARGA system, the airflow enters the equipment at a constant rate of 1 m^3 h^{-1} via a Teflon-coated inlet, with a cut-off for particles smaller than 10 μm (PM_{10}). The gas-phase compounds are collected by a WRD (wet rotating denuder) whereas the particulate matter passes through the WRD to be collected subsequently by a SJAC (Steam-Jet Aerosol Collector). For more information about the MARGA system we refer the reader to ten Brink et al. (2007) and Thomas et al. (2009). The NO_X-O_3 observations were taken at the nearby RIVM station (National Institute for Public Health and the Environment – www.lml.rivm.nl) in Zegveld, located at 20 km from the CESAR site. The aerosol optical depth was taken from the AERONET Level 1.5 data for Cabauw. The single scattering albedo was taken from the AERONET inversion data.

2.3. Experimental design

Barbaro et al. (2014) showed that during the morning CESAR2008 is characterized by a distinctive 1500 m residual layer (RL) sitting above a strong surface inversion (located at around 200 m above the surface). They also showed that the well-mixed vertical structure of the RL allows a very rapid growth of the CBL after the break up of the morning inversion. During the afternoon the CBL grows fairly little (at a rate of ≈60 m h^{-1}) and the thermodynamical conditions remain relatively constant. Based on this, and similar to Aan de Brugh et al. (2013), we focus only on the afternoon period (11-16 UTC), which shows little CBL growth. We use as initial conditions the (thermo)dynamics, radiation and land-surface fields obtained by Barbaro et al. (2014) at 11 UTC.

Due to the computational cost of this coupled-LES experiment, the spatial numerical domain that has been simulated is reduced to 4800 × 4800 × 3000 m aiming to maintain the same spatial resolution of 50 × 50 × 15 m as in Barbaro et al. (2014). We verified that results are almost identical despite the reduction in the horizontal domain (not shown). We assume in the domain periodic horizontal boundary conditions, and to prevent numerical instabilities due to the chemical differential equations we reduced the original time step from 3 s to 1 s throughout the whole simulation.

In Aan de Brugh et al. (2013) an effective equilibration timescale of 30 min was adopted. Following their results, and the good agreement with observations (discussed in Sect. 3) we also adopt a constant (with respect to time and height) effective aerosol equilibration timescale of 30 min. Note, however, that based exclusively on the aerosol properties described in Sect. 2.1.2, a mass accommodation coefficient for aerosol nitrate equal to 0.5 (Dassios and Pandis, 1999), and a particle number concentration of 1000 cm^{-3} (Hamburger et al., 2011) we calculate a τ_{eq} of approximately 3.5 min (see Eq. (3) in Saleh et al. (2013)). A plausible explanation for the difference between the calculated and effective τ_{eq} is that other chemical species (e.g. viscous secondary organic aerosols), may increase τ_{eq} due to aerosol mass-transport limitation (Morino et al., 2006; Shiraiwa and Seinfeld, 2012). Additionally, the larger ammonium nitrate particles in the mode adapt slowest to the new environmental thermodynamics (Saleh et al., 2013), and therefore also augment τ_{eq}. The use of a larger τ_{eq} might also account for the

complex relation between chemistry and the multiscale character of CBL turbulence and thermodynamics (Morino et al., 2006). In the CBL, smaller eddies alter the local environment at the scale of individual particles, whereas larger eddies transport the aerosols to different thermodynamic conditions within the entire CBL. These processes are characterized by different timescales, and combined may result in a larger τ_{eq}. The explanation of a larger τ_{eq} is similar to the larger turbulent timescale compared to the Kolmolgorov timescale, affecting cloud droplet formation (Grabowski and Wang, 2013).

In the setup used by Barbaro et al. (2014), τ and ω were prescribed following the observations taken during the EUCAARI campaign. Here we use the aerosol module (Sect. 2.1.2) coupled to our LES to explicitly calculate these aerosol properties for every time step based on the aerosol concentrations of black carbon, ammonium, nitrate, sulfate and aerosol water. As shown later, our τ and ω are in close agreement with the observations and the LES results discussed in Barbaro et al. (2014).

We impose for CESAR2008 a constant surface emission of NO_X equal to 0.23 ppb m s^{-1} to account for the highway emission nearby the CESAR site. Most of the NO_X emissions in the Netherlands are vehicular (Velders et al., 2011), and 90% (10%) are assumed to be in the form of NO (NO_2). Our NH_3 surface exchange is modeled as a combination of typical spring emission and deposition, and amounts, on average during the day, to 0.38 ppb m s^{-1}. This value agrees with flux measurements taken at Cabauw (on average $\approx$0.3 ppb m s^{-1}) see Erisman et al. (1989). We use a constant small isoprene surface emission equal to 15 ppt m s^{-1} to account for advection of nearby forested areas, leading to mixing ratios around 30 ppt within the CBL. The CH_4 and CO initial mixing ratios are set equal to 1.8 ppm and 0.2 ppm, respectively. These values are in agreement with climatological observations taken at CESAR (Vermeulen et al., 2011). We summarize the initial concentrations (CBL and free-troposphere) and surface fluxes (emission/deposition velocity) of the most important chemicals in Table 1.

In addition to the CESAR2008 experiment we design another LES experiment prescribing the same boundary-layer and surface properties as CESAR2008 but shortening the equilibration timescale to 10 min (hereafter called CESAR2008-10). Our motivation is that the microphysical properties of aerosol nitrate have not been measured at Cabauw during CESAR2008, and the equilibration timescale plays a crucial role in the vertical transport of nitrate and on partitioning of TNO_3 within the CBL (Dassios and Pandis, 1999; Morino et al., 2006; Aan de Brugh et al., 2012). The 10-min equilibration timescale is also closer to the value of 3.5 min, calculated according to Saleh et al. (2013). By performing these numerical experiments, we cover the situations where the turbulent time scale ($\tau_T \approx 17$ min) is either slightly longer or slightly shorter than the equilibration time scale. Therefore, strong interactions between gas-aerosol conversion and turbulence are expected (Fitzjarrald and Lenschow, 1983; Vinuesa and Vilà-Guerau de Arellano, 2003; Aan de Brugh et al., 2012).

We use the WUSCM to investigate the ability of a non-eddy resolving model to reproduce our horizontally-averaged LES fields for the CESAR2008 experiment. In the WUSCM we use the same setup as in the work by Aan de Brugh et al. (2012). Similarly, the Medium Range Forecast (MRF) scheme is used to calculate the boundary-layer diffusion (Troen and Mahrt, 1986; Hong and Pan, 1996), and the momentum calculations are based on the parametrization proposed by Noh et al. (2003). To ensure consistency in the comparison between LES-averaged fields and the WUSCM vertical profiles, both the WUSCM and the LES model use the same free-tropospheric initial concentrations for ammonium nitrate and ammonium sulphate (Table 1). Besides that, the initial conditions for the (thermo)dynamics, land-surface, and net-radiation used in the WUSCM are taken from Barbaro et al. (2014). Also similarly to Aan de Brugh et al. (2012), the time step adopted in the WUSCM is 20 s. Note that reducing the time step in the WUSCM did not alter the results discussed here (not shown).

Table 1
Boundary conditions and initial concentrations at the CBL and free-troposphere for the CESAR2008 experiment. The v_d values are dynamically calculated depending on the resistances but remain fairly constant during the whole simulation. Note the free-tropospheric values for black carbon, ammonium nitrate, and ammonium sulfate used to compensate for the lack of organic aerosol in our model. Also note that aerosol ammonium (NH_4^+) is formed by neutralization of H_2SO_4 and HNO_3.

Chemicals	Surface		CBL (ppb)	FT (ppb)
	Emission (ppb m s^{-1})	v_d (cm s^{-1})		
NO	0.21	0.10	1.0	0.1
NO_2	0.02	0.45	4.0	1.0
O_3	–	0.60	57	65
Isoprene	0.015	–	0.01	0.01
BC	–	0.004	1.5	1.5
$^gHNO_3$	–	1.86	0.9	0.9
$^ANO_3$	–	0.004	2.0	2.3
SO_4^{2-}	–	0.004	1.3	1.3
NH_3	0.5	1.01	11	1.0
NH_4^+	–	0.004	4.6	4.9
CH_4	–	–	1800	1800
CO	–	0.002	200	200

3. Evaluation of our LES results against surface observations

As described in the experimental design section, the initial conditions for (thermo)dynamics and radiation used in our LES are taken from Barbaro et al. (2014). Therefore, here we omit the evaluation of radiation and surface energy budgets, CBL height (based on the minimum of the buoyancy flux), and thermodynamics (potential temperature and specific humidity), which are shown in Fig. 3 of Barbaro et al. (2014). The evolution of the temperature and relative humidity at 2 m height is shown in Fig. 1 of Aan de Brugh et al. (2013). In Fig. 1 we present an evaluation of the CBL chemistry and the aerosol properties against the available surface observations. The results correspond to an aerosol equilibration time partitioning equal to 30 min (Aan de Brugh et al., 2013). Note that we concentrate our analysis only in the afternoon CBL to reduce the role of diurnal variability (Barbaro et al., 2014). The observations of ozone, NO_X, gas-aerosol nitrate and ammonia taken at CESAR are hourly averaged.

Based on Fig. 1 we conclude that our LES is able to adequately simulate the chemistry and the aerosol properties during the afternoon for CESAR2008. It can be observed that the NO_X-O_3 is well reproduced. Comparable O_3 mixing ratios during the afternoon are commonly observed in CESAR (Demuzere et al., 2009) and similar NO_X-O_3 mixing ratios were recently reported throughout the whole Europe during the PEGASOS campaign (Jager, 2014). The $^gHNO_3$ and $^ANO_3$ concentrations are also properly simulated in our LES (adopting a constant equilibration time scale equal to 30 min). The TNO_3 partitioning, defined as $^gHNO_3/(^gHNO_3 + {}^ANO_3)$, is also well in agreement with the surface observations, with a diurnal average overestimation of $\approx$12%. This result supports the use of the effective equilibration timescale equal to 30 min to simulate the partitioning of nitrate within the CBL for this case. Note, however, that the chemistry of the CESAR2008 case is characterized by a small diurnal variability (specially for NO_X-O_3). Therefore, the good match obtained with our LES framework compared to the surface observations is partly explained by our choice of initial concentrations (shown in Table 1).

The elevated NH_3 concentrations within the CBL (Fig. 1g) are explained by the high surface emissions due to the intense cattle

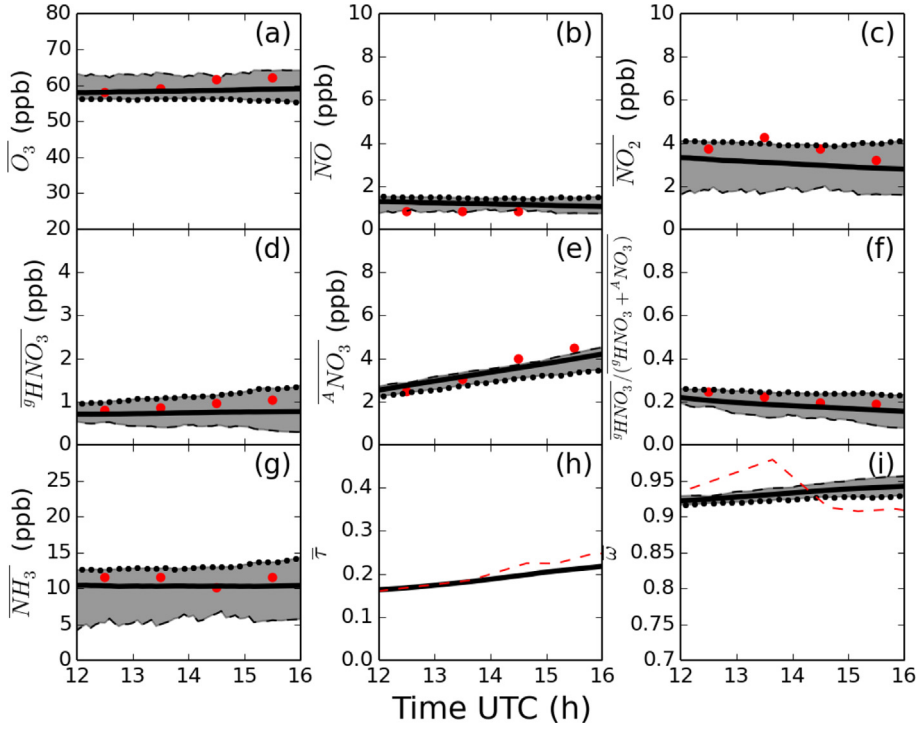

Fig. 1. Time evolution of the chemistry (a–g) and aerosol properties (h–i) for our LES framework (CESAR2008) and surface observations taken at CESAR. The red dots represent the RIVM/CESAR hourly-averaged surface observations and the red dashes the EUCAARI continuous aerosol measurements (at 550 nm). The shades represent the difference between the horizontally-averaged values at the surface (black dots) and at the top of the CBL (dashes). The black lines represent the bulk values of the atmospheric compounds averaged over the CBL. (For interpretation of the references to color in this figure legend, the reader is referred to the web version of this article.)

farming in the Netherlands (Velthof et al., 2012). The significant differences between the maximum–minimum (shades) concentrations observed for NH_3 are due to surface emissions and the small free-tropospheric concentrations (the latter also seen for NO_2) compared to the surface values (see Table 1). The fluctuations observed at the top of the CBL (dashes) are due to entrainment of cleaner air from the free-troposphere.

The aerosol properties are well reproduced during the whole simulation. Around 13.5 UTC advection of polluted air brings slightly more absorbing aerosols from Central Europe (Hamburger et al., 2011), decreasing ω. Nevertheless, the aerosol optical depth remains almost unchanged. We are able to compensate for the lack of organic aerosol in our model and therefore to properly reproduce τ by adding ammonium nitrate and sulfate, and black carbon in the free atmosphere. We are aware that this may lead to excessive entrainment of aerosols from the free-troposphere. However, the CBL grows fairly little during the whole simulated period.

4. Impact of different equilibration timescales on the gas-aerosol conversion

In Fig. 2 we compare the vertical profiles of gas-phase and aerosol nitrate, total nitrate and ammonia obtained for CESAR2008 ($\tau_{eq} = 30$ min) and CESAR2008-10 ($\tau_{eq} = 10$ min) experiments. To ensure robustness, all the vertical profiles are horizontally- and time-averaged between 12.5 UTC − 14.5 UTC.

We observe in Fig. 2 that the gas-aerosol conversion mechanisms and the equilibration timescale significantly influence the vertical profiles of ${}^gHNO_3$ and ${}^ANO_3$ for both numerical experiments. Regardless of the well-mixed character of the CBL, more ${}^gHNO_3$ is observed at the surface if compared with the top of the CBL. As expected, we note the opposite for ${}^ANO_3$.

We observe steeper gradients in the vertical profiles of gas-aerosol nitrate for the shorter equilibration time scale. This is explained by the faster gas-aerosol conversion. In that case, the

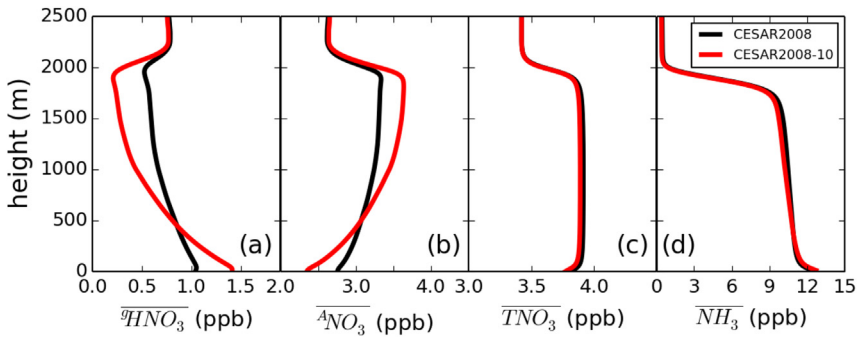

Fig. 2. Horizontally-averaged vertical profiles of (a) ${}^gHNO_3$ (b) ${}^ANO_3$ (c) TNO_3 (d) NH_3. The legend indicates the experiment.

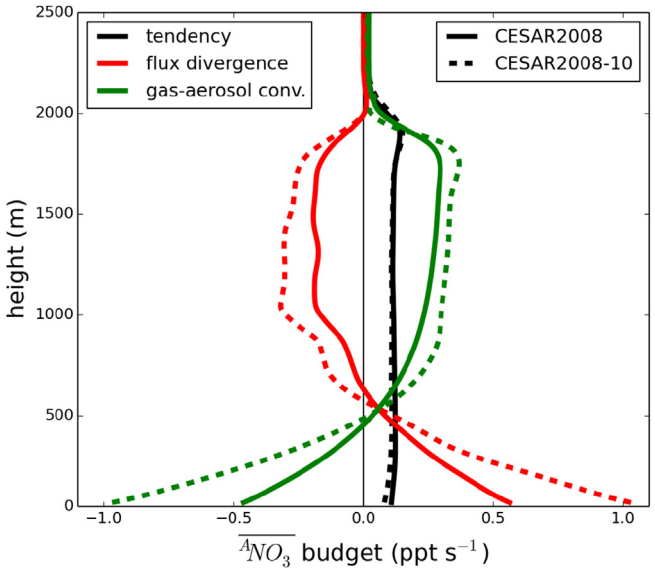

Fig. 3. Vertical profile of the $^{A}NO_3$ budget time-averaged between 12.5UTC − 14.5UTC. The budget terms and the experiments are indicated in the legends.

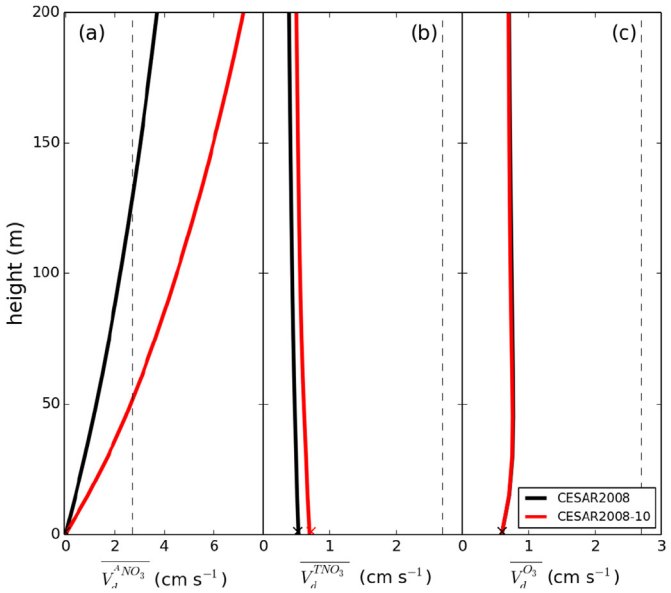

Fig. 5. Vertical profiles of the deposition velocity calculated by our LES within the surface layer for (a) $^{A}NO_3$ (b) TNO_3 and (c) O_3. The thin dashed-lines refer to the maximum possible deposition velocity $v_d = 1/r_a$. The crosses refer to the deposition velocities calculated at the surface (Table 1). The deposition velocity for TNO_3 is explained in the text. The profiles are time-averaged between 12.5UTC − 14.5UTC. The different experiments are indicated in the legend.

equilibration time scale is shorter than the boundary-layer time scale ($\tau_T \approx 17$ min), creating a gradient that is maintained due to the relative slow turbulent motions. Note that more gas-phase nitrate is present close to the surface for the shorter equilibration timescale. That leads to higher values of TNO_3 partitioning at the surface, which is less consistent with observations (Fig. 2a and b, and Fig. 1f).

Since $^{g}HNO_3$ is converted into $^{A}NO_3$ and vice-versa, we note in Fig. 2c that the TNO_3 vertical profile is similar to a conserved variable. The small difference for the TNO_3 vertical profile between the two experiments is explained by larger quantities of $^{g}HNO_3$ close to the surface for CESAR2008-10 (Fig. 2a). In that case, more nitric acid deposits and by consequence the TNO_3 is slightly smaller than for CESAR2008. A well-mixed character is observed for NH_3 (Fig. 2d). Close to the surface and near the top of the CBL the profile is influenced by emission/deposition and detrainment, respectively. Due to the abundance of NH_3 we note that its association with $^{g}HNO_3$ has only a minor influence on its vertical distribution.

We present in Fig. 3 the $^{A}NO_3$-budget calculated based on Eq. (1). This budget quantifies the vertical contributions of (i) turbulent flux divergence and (ii) gas-aerosol conversion of nitrate to the tendency of $^{A}NO_3$ within the CBL.

Gas-aerosol conversion and vertical divergence of the turbulent flux contribute oppositely to the $^{A}NO_3$ evolution within the CBL. Close to the surface, aerosol nitrate outgasses to $^{g}HNO_3$ and a strong positive $^{A}NO_3$ vertical gradient is created. From the mid-CBL up to the top of the CBL, downdrafts rich in $^{A}NO_3$ act towards homogenizing the $^{A}NO_3$ profile. As a net effect, the tendency term is positive and approximately constant with height indicating that aerosol nitrate is being produced throughout the CBL (see Fig. 1e).

As also shown by Aan de Brugh et al. (2012), reducing the equilibration timescale increases the contribution of the gas-aerosol conversion to the budget. Accordingly, the turbulent term reacts proportionally, implying in a larger turbulent vertical flux. Therefore, we show in Fig. 4 the influence of the equilibration timescale on the vertical profiles of the turbulent fluxes for the same variables discussed in Fig. 2.

The vertical fluxes for both $^{g}HNO_3$ and $^{A}NO_3$ are highly nonlinear, driven by the spatial distributions of absolute temperature and relative humidity. Both maxima occur at around 1/3 of the CBL (Aan de Brugh et al., 2013). In accordance to the vertical profiles of these concentrations (Fig. 2) the fluxes are larger for the shorter equilibration timescale. Since $^{g}HNO_3$ is converted into $^{A}NO_3$ and vice-versa, the turbulent fluxes for both variables are opposite and

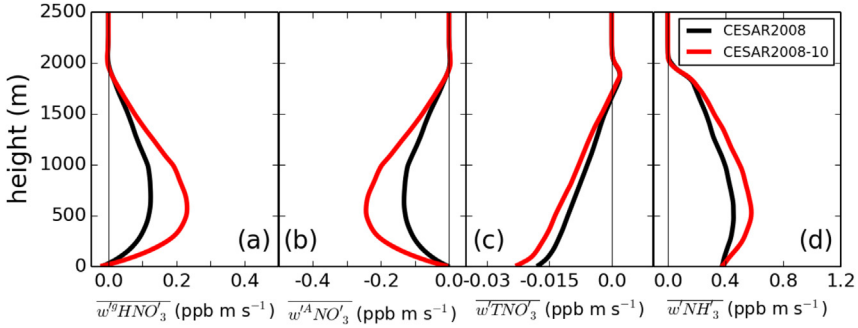

Fig. 4. Same as Fig. 2 but for the turbulent vertical fluxes.

almost equal in magnitude. The small negative flux for total nitrate is caused by ${}^{g}HNO_3$ deposition since ${}^{A}NO_3$ deposition velocities are very small. As presented in Table 1, the net-turbulent flux of NH_3 depends on dry deposition and surface emission.

5. Aerosol nitrate deposition velocity

In our LES, we are able to explicitly calculate a height-dependent deposition velocity by taking the ratio between the turbulent vertical flux and the mean concentration at the surface (see SM). We compare these velocities with the deposition velocities calculated at the surface based both on the atmospheric and surface resistances (see Table 1). We show in Fig. 5 the deposition velocities for ${}^{A}NO_3$, TNO_3 and O_3 within the surface layer for the CESAR2008 and CESAR2008-10 experiments.

We notice in Fig. 5a that $v_d^{{}^{A}NO_3}$ increases significantly with height within the surface layer and becomes even larger than the maximum deposition velocity – defined as the inverse of the atmospheric resistance (Ganzeveld and Lelieveld, 1995). The strong vertical gradient observed within the surface layer explains why several observational studies have reported significant deposition velocities for aerosol nitrate (see Hanson (1991) for an extensive review). This overestimation of the deposition velocity (known as "apparent deposition") is caused by the strong outgassing of ${}^{A}NO_3$ close to the surface (Huebert et al., 1988; Nemitz and Sutton, 2004). Comparing our LES experiments we find that this effect becomes more important at shorter time scales since the outgassing of ${}^{A}NO_3$ becomes more efficient. We found in Fig. 5b a larger TNO_3 deposition velocity for the CESAR2008-10 experiment (0.75 cm s^{-1}) compared to the CESAR2008 experiment (0.56 cm s^{-1}). This is explained by the fact that the TNO_3 deposition velocity is calculated by a concentration-weighted average between aerosol nitrate and gas phase nitrate deposition velocities (Morino et al., 2006). In Fig. 5c the nearly constant deposition velocity throughout the surface layer is in agreement with the calculated value at the surface for O_3 (0.6 cm s^{-1}).

The ${}^{A}NO_3$ turbulent flux within the surface layer varies significantly with height. This indicates that the deposition velocity for ${}^{A}NO_3$ cannot be calculated using measurements of ${}^{A}NO_3$ made too far away from the surface (Fitzjarrald and Lenschow, 1983; Wolff et al., 2010). The results shown in Fig. 5 for ${}^{A}NO_3$ deposition have implications from the measurement perspective. For example, ${}^{A}NO_3$ deposition velocities measured at around 30 m height can be of the order of 2 cm s^{-1} depending on the equilibration time scale. To avoid that issue, we suggest the calculation of the deposition velocity for TNO_3 instead, since it can be treated as a conservative quantity, as shown in Fig. 5b. Our conclusion agrees with the observations presented by Huebert et al. (1988) and Wolff et al. (2010). For ${}^{g}HNO_3$, Huebert and Robert (1985) found a daytime average deposition velocity equal to 2.5 ± 0.9 cm s^{-1} under similar temperature and land-surface conditions. This value is comparable to $v_d^{{}^{g}HNO3} = 1.9$ cm s^{-1} we calculated for our LES simulations. Our values are also within the range found by Nemitz et al. (2004). For NH_3, the calculated deposition velocity ($v_d^{NH_3} = 1.0$ cm s^{-1}) is also well within the range obtained by Hesterberg et al. (1996) for grassland. The calculated ozone deposition velocity (0.6 cm s^{-1}) agrees with the ones obtained by Meszaros et al. (2009) in terms of observations (0.44 ± 0.23 cm s^{-1}) and modeling (0.52 ± 0.08 cm s^{-1}) over grassland.

Our vertical resolution (15 m) suffices to capture the most important physical processes controlling the deposition process and interactions between surface and turbulence. Despite that, detailed higher resolution numerical studies, e.g. Nemitz and Sutton (2004) remain crucial to study the outgassing of nitrate aerosol close to the surface.

6. Representation of the transport of aerosol nitrate within the CBL

As shown in Figs. 2 and 4, the vertical distribution of aerosol nitrate depends on absolute temperature and on fluctuations with respect to the vertical velocity. In consequence, the turbulent transport of the aerosol nitrate (first term on the rhs in Eq. (1)) might be influenced by the gas-aerosol conversion. This may affect the representation of the vertical turbulent flux of nitrate in 1D models. Our LES is used here (i) to explicitly resolve all the terms of the horizontally-averaged flux budget equation for aerosol nitrate, and (ii) to help us derive a new parameterization for the turbulent flux of aerosol nitrate (see Sects. 2 and 3 in the SM).

In short, the results indicate that the ${}^{A}NO_3$ flux remains in steady-state because the transport of ${}^{A}NO_3$ and chemistry contributions are in close balance with the buoyancy term and production of ${}^{A}NO_3$ flux. Specially, the buoyancy term remains important within the entire CBL, and cannot be ignored. This is explained by the fact that the ${}^{A}NO_3$ flux depends not only on the turbulent transport, but also on the temperature dependent gas-aerosol conversion. Therefore, we ask ourselves whether the traditional representation (i.e. inert K-theory) of the turbulent flux is still valid for aerosol nitrate since this species explicitly depends on the CBL thermodynamics and on the equilibration timescale. To answer that question, we extend earlier research (Vilà-Guerau de Arellano and Duynkerke, 1992; Hamba, 1993; Verver, 1994; Vinuesa and Vilà-Guerau de Arellano, 2003) and propose here to calculate an exchange coefficient for ${}^{A}NO_3$. We do that by adding to the exchange coefficient for heat the effects of the gas-aerosol equilibration timescale and absolute temperature. The detailed derivation is given in the SM. In Eq. (2) we show the proposed expression to close the turbulent flux of ${}^{A}NO_3$:

$$\overline{w'{}^{A}NO_3'} = -K_{{}^{A}NO_3}\frac{\partial \overline{{}^{A}NO_3}}{\partial z}$$
$$K_{{}^{A}NO_3} = K_H\frac{\tilde{B}}{\tilde{C}}, \tag{2}$$

where $K_{{}^{A}NO_3}$ is the inert exchange coefficient for heat (K_H) depending not only on turbulent characteristics but also on chemistry ($\tilde{C}$) and gas-aerosol conversion of nitrate ($\tilde{B}$). The chemistry term $\tilde{C}$ is equal to $(1 + 2Da)$, where Da is the Damköhler number, which relates the turbulent timescale to the chemical timescale (see SM). Note that for very slow chemistry ($Da \ll 1$) this term vanishes from the equation. In our case (Da $\approx$ 1) and chemistry tends to make $K_H > K_{{}^{A}NO_3}$. The physical meaning is that during the turbulent transport of the air parcel, the species are reacting and in consequence the exchange coefficient becomes smaller (Vilà-Guerau de Arellano and Duynkerke, 1992). The buoyant correction term $\tilde{B}$ (see SM) depends on a positive closure term adjustable to the LES results, and remains always positive. Consequently, $\tilde{B}$ tends to make $K_{{}^{A}NO_3} > K_H$. The interpretation of a larger exchange coefficient is that for an adequate representation of the nitrate turbulent flux we need a larger characteristic mixing length scale that accounts not only the turbulent transport, but also for the temperature dependent gas-aerosol conversion of nitrate.

We evaluate the new exchange coefficient calculated using Eq. (2) by comparing the horizontally-averaged LES nitrate fields with the WUSCM nitrate profiles calculated with the new $K_{{}^{A}NO_3}$ profiles for the CESAR2008 case. We also examine the impact of the new exchange coefficient on the gas-aerosol partitioning of nitrate at the surface. Note that for long-lived species (i.e. Da $\gg$ 1) and thermodynamic variables (e.g. θ) there is enough time for the turbulent eddies to mix the properties within the CBL. In these cases, (horizontally-averaged) well-mixed vertical distributions within

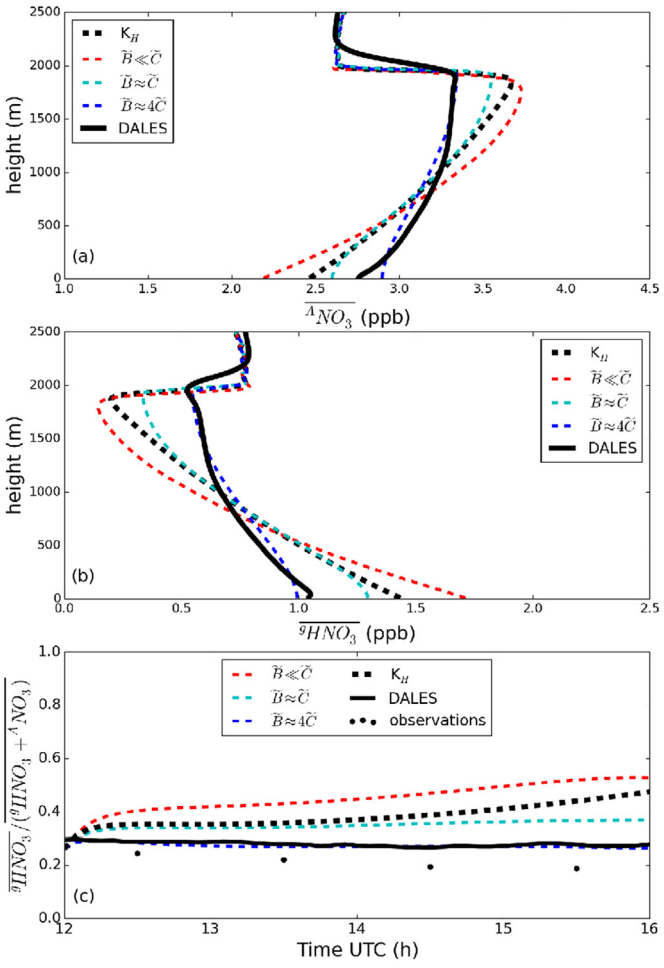

Fig. 6. Vertical profiles of (a) ${}^{A}NO_3$ and (b) ${}^{g}HNO_3$ obtained by the LES (continuous lines) and the WUSCM (dashes) for different corrections time-averaged between 12.5UTC − 14.5UTC. (c) Time evolution of the TNO_3 partitioning at the surface. The colored-dashes indicate the different corrections used in the WUSCM.

the CBL are observed. Since the same boundary and initial conditions are used in the WUSCM and the LES model, the vertical profiles of long-lived species calculated by both models remain very similar throughout the entire simulation.

We notice in Fig. 6 that the use of K_H leads to an under(over) estimation of ${}^{A}NO_3$ (${}^{g}HNO_3$) close to the surface. Also, the comparison between LES and WUSCM profiles worsens for the chemistry correction much larger than the buoyant correction (i.e. $\tilde{B}\ll\tilde{C}$). This is because the chemistry solely tends to decrease the exchange coefficient and as a consequence, the vertical gradients tend to increase. In contrast, the effect of buoyancy enlarges the exchange coefficient, enhancing vertical mixing. Absolute temperature (decreases with height in the CBL) and aerosol nitrate (increases with height in the CBL) are anti-correlated, leading to a positive $\tilde{B}$ term (see SM). As a consequence, the vertical gradients for both gas-phase and aerosol nitrate diminish. We found the best match between LES and WUSCM for $\tilde{B}/\tilde{C}\approx 4$. Accordingly, the TNO_3 partitioning at the surface obtained by the WUSCM progressively approaches the LES values resulting in a better agreement with the observations taken at CESAR as the ratio $\tilde{B}/\tilde{C}$ increases.

Our intent here is to show that the impact of the temperature-dependent gas-aerosol conversion of nitrate in the buoyant term has a non-negligible effect on the vertical transport of nitrate (Verver, 1994). We alert the reader that different CBL thermodynamics and gas-aerosol equilibration timescale may alter the magnitude of the ratio $\frac{\tilde{B}}{\tilde{C}}$ found here. Future studies should therefore aim to extend this result, for example for warmer/cooler CBLs, as also discussed in Aan de Brugh et al. (2013).

7. Conclusions

We studied the transport and formation of ammonium nitrate aerosol within the convective boundary layer (CBL) using a large-eddy simulation (LES) in which radiation, aerosols, CBL dynamics and surface processes are coupled in the same framework. Our LES model was successfully evaluated against observations of chemistry and aerosol fields. We performed a sensitivity analysis on the impact of a shorter and a larger equilibration timescale compared to the characteristic turbulent time scale on the gas-aerosol conversion of nitrate within the CBL. Our LES results indicated that 30 min is an adequate equilibration timescale of nitrate for this case. We noted that the vertical distribution of gas-aerosol nitrate showed a significantly larger variability for shorter equilibration timescales, despite the well-mixed nature of the CBL.

Using our LES we quantified the effect of gas-aerosol conversion on the nitrate deposition flux within the surface layer. Our results confirmed that the large deposition velocities for aerosol nitrate close to the surface are due to outgassing. As a consequence, the total nitrate deposition flux depends on the gas-phase nitrate concentration at the surface. We found that a shorter equilibration timescale resulted in a larger deposition velocity of total nitrate.

We found using our LES that the mixing between poor-nitrate updrafts (warm) and rich-nitrate downdrafts (cold) within the CBL significantly altered the vertical turbulent flux of gas-aerosol nitrate. The maximum of the gas-aerosol nitrate vertical flux was located at $\approx 1/3$ of the CBL height. The turbulent flux of aerosol nitrate was also influenced by the interaction between CBL dynamics and chemistry. The LES provided us with a framework to interpret the vertical profiles of gas-aerosol nitrate obtained by a 1D model. Based on the LES results, we proposed a new formulation to parameterize the turbulent flux of nitrate in the 1D model. The results indicated the need to increase the exchange coefficient used in non-eddy resolving models to better account for the complex interaction between gas-aerosol conversion of nitrate and turbulence within the CBL. Indeed, the new exchange coefficient also improved the comparison between gas-aerosol partitioning of nitrate calculated with our 1D model and surface observations.

Our findings indicate that to understand the evolution of gas-aerosol nitrate in the boundary layer, it is necessary to solve and represent simultaneously the CBL (thermo)dynamics, surface exchange processes, and gas-aerosol conversion of nitrate. Under this framework we were able to better interpret observations of nitrate deposition velocity close to the surface, and also to augment our understanding about the relation between turbulent transport and gas-aerosol conversion of nitrate.

Acknowledgments

We are grateful to Henk Klein Baltink and Fred Bosveld for the CESAR data set (www.cesar-database.nl). E. Barbaro thanks Joost Aan de Brugh, Wayne Angevine, Bert Holtslag, Arnold Moene, and Edward Patton for very useful discussions on the results of this work. This research is supported by the EU FP7 IP PEGASOS (FP7-ENV-2010/265148) and by the NWO grant for computing time (SH-060-14). Finally, we gratefully thank the two anonymous reviewers for their helpful comments that contributed to improving this manuscript.

Appendix A. Supplementary data

Supplementary data related to this article can be found at http://dx.doi.org/10.1016/j.atmosenv.2015.01.048.

References

Aan de Brugh, J.M.J., Henzing, J.S., Schaap, M., Morgan, W.T., van Heerwaarden, C.C., Weijers, E.P., Coe, H., Krol, M.C., 2012. Modelling the partitioning of ammonium nitrate in the convective boundary layer. Atmos. Chem. Phys. 12 (6), 3005–3023. http://dx.doi.org/10.5194/acp-12-3005-2012.

Aan de Brugh, J.M.J., Ouwersloot, H.G., Vilà-Guerau de Arellano, J., Krol, M.C., 2013. A large-eddy simulation of the phase transition of ammonium nitrate in a convective boundary layer. J. Geophys Res. Atmos. 118 (2), 826–836. http://dx.doi.org/10.1002/jgrd.50161.

Angevine, W.M., Grimsdell, A.W., Mckeen, S.A., 1998. Entrainment results from the FLATLAND boundary layer experiments. J. Geophys Res. 103 (98), 13,689–13,701. http://dx.doi.org/10.1029/98JD01150.

Baklanov, A., Schlunzen, K., co authors, 2014. Online coupled regional meteorology chemistry models in europe: current status and prospects. Atmos. Chem. Phys. 14 (1), 317–398.

Barbaro, E., de Arellano, J.V.-G., Ouwersloot, H.G., Schrter, J.S., Donovan, D.P., Krol, M.C., 2014. Aerosols in the convective boundary layer: shortwave radiation effects on the coupled land-atmosphere system. J. Geophys. Res. Atmos. 119 (10), 5845–5863. http://dx.doi.org/10.1002/2013JD021237.

Bellouin, N., Boucher, O., Haywood, J., Reddy, M.S., 2005. Global estimate of aerosol direct radiative forcing from satellite measurements. Nature 438 (7071), 1138–1141.

Dassios, K.G., Pandis, S.N., 1999. The mass accommodation coefficient of ammonium nitrate aerosol. Atmos. Environ. 33 (18), 2993–3003.

Demuzere, M., Trigo, R.M., Vilà-Guerau de Arellano, J., van Lipzig, N.P.M., 2009. The impact of weather and atmospheric circulation on O3 and PM10 levels at a rural mid-latitude site. Atmos. Chem. Phys. 9, 2695–2714.

Dusek, U., ten Brink, H., Meijer, H., Kos, G., Mrozek, D., Röckmann, T., Holzinger, R., Weijers, E., 2013. The contribution of fossil sources to the organic aerosol in the Netherlands. Atmos. Environ. 74, 169–176. http://dx.doi.org/10.1016/j.atmosenv.2013.03.015.

Erisman, J., De Leeuw, F.A.A.M., Van Aalst, R.M., 1989. Deposition of the most acidifying components in the netherlands during the period 1980-1986. Atmos. Environ. 23 (5), 1051–1062.

Fitzjarrald, D.R., Lenschow, D.H., 1983. Mean concentration and flux profiles for chemically reactive species in the atmospheric surface layer. Atmos. Environ. 17 (12), 2505–2512.

Fountoukis, C., Nenes, A., 2007. ISORROPIAII: a computationally efficient thermodynamic equilibrium model for K+ Ca2+ Mg2+ NH4+ Na+ SO42- NO3- Cl- H2O aerosols. Atmos. Chem. Phys. 7 (17), 4639–4659.

Ganzeveld, L., Lelieveld, J., 1995. Dry deposition parameterization in a chemistry general circulation model and its influence on the distribution of reactive trace gases. J. Geophys. Res. 100 (D10), 20,999–21,012.

Grabowski, W.W., Wang, L.-P., 2013. Growth of cloud droplets in a turbulent environment. Annu. Rev. Fluid Mech. 45 (1), 293–324. http://dx.doi.org/10.1146/annurev-fluid-011212-140750.

Hamba, F., 1993. A modified K model for chemically reactive species in the planetary boundary layer. J. Geophys. Res. 98-D3 (92), 5173–5182.

Hamburger, T., McMeeking, G., Minikin, a., Birmili, W., Dall'Osto, M., O'Dowd, C., Flentje, H., Henzing, B., Junninen, H., Kristensson, a., de Leeuw, G., Stohl, a., Burkhart, J.F., Coe, H., Krejci, R., Petzold, a., 2011. Overview of the synoptic and pollution situation over Europe during the EUCAARI-LONGREX field campaign. Atmos. Chem. Phys. 11 (3), 1065–1082. http://dx.doi.org/10.5194/acp-11-1065-2011.

Hanson, P.J., 1991. Dry deposition of reactive nitrogen compounds: a review of leaf, canopy and non-foliar measurements. Atmos. Environ. 25A (8).

Harrison, R.M., Pio, C.A., 1983. An investigation of the atmospheric HNO3-NH3-NH4NO3 equilibrium relationship in a cool, humid climate. Telus 35B, 155–159.

Hesterberg, R., Blatter, A., Fahrni, M., Rosset, M., Neftel, A., Eugster, W., Wanner, H., 1996. Deposition of nitrogen-containing compounds to an extensively managed grassland in central switzerland. Environ. Pollut. 91 (1), 21–34.

Heus, T., van Heerwaarden, C.C., Jonker, H.J.J., Siebesma, A.P., Axelsen, S., van den Dries, K., Geoffroy, O., Moene, A., Pino, D., de Roode, S.R., Vilà-Guerau de Arellano, J., 2010. Formulation of the Dutch atmospheric Large-Eddy simulation (DALES) and overview of its applications. Geosci. Model Dev. 3, 415–444.

Hong, S.-Y., Pan, H.-L., 1996. Nonlocal boundary layer vertical diffusion in a medium-range forecast model. Mon. Wea. Rev. 124 (10), 2322–2339.

Huebert, B., Robert, C., 1985. The dry deposition of nitric acid to grass. J. Geophys. Res. 90, 2085–2090.

Huebert, B.J., Luke, W.T., Delany, A.C., Brost, R.A., 1988. Measurements of concentrations and dry surface fluxes of atmospheric nitrates in the presence of ammonia. J. Geophys. Res. 93 (D6), 7127–7136.

Huijnen, V., Williams, J., Van Weele, M., Van Noije, T., Krol, M., Dentener, F., Segers, A., Houweling, S., Peters, W., De Laat, J., Boersma, F., Bergamaschi, P., Van Velthoven, P., Le Sager, P., Eskes, H., Alkemade, F., Scheele, R., Ndlec, P., Ptz, H., 2010. The global chemistry transport model tm5: description and evaluation of the tropospheric chemistry version 3.0. Geosci. Model Dev. 3 (2), 445–473.

Jacobson, M.Z., 1998. Studying the effects of aerosols on vertical photolysis rate coefficient and temperature profiles over an urban airshed. J. Geophys Res. 103.

Jager, J.E., 2014. Airborne VOC Measurements on Board the Zeppelin NT during the PEGASOS Campaigns in 2012 Deploying the Improved Fast-GC-MSD System. Forschungszentrum Julich GmbH, Germany, p. 182.

Jiang, H., Feingold, G., 2006. Effect of aerosol on warm convective clouds: aerosol-cloud-surface flux feedbacks in a new coupled large eddy model. J. Geophys. Res. 111 (D1), D01,202. http://dx.doi.org/10.1029/2005JD006138.

Kaufman, Y., Tanr, D., Boucher, O., 2002. A satellite view of aerosols in the climate system. Nature 419, 215–223.

Krol, M., Houweling, S., Bregman, B., van den Broek, M., Segers, A., van Velthoven, P., Peters, W., Dentener, F., Bergamaschi, P., 2005. The two-way nested global chemistry-transport zoom model TM5: algorithm and applications. Atmos. Chem. Phys. 5, 417–432. http://dx.doi.org/10.5194/acp-5-417-2005.

Krol, M.C., Molemaker, M.J., Vilà-Guerau de Arellano, J., 2000. Effects of turbulence and heterogeneous emissions on photochemically active species in the convective boundary layer. J. Geophys. Res. 105, 6871–6884. http://dx.doi.org/10.1029/1999JD900958.

Kulmala, M., Asmi, A., co authors, 2011. General overview: European integrated project on aerosol cloud climate and air quality interactions (EUCAARI) integrating aerosol research from nano to global scales. Atmos. Chem. Phys. 11 (24), 13,061–13,143. http://dx.doi.org/10.5194/acp-11-13061-2011.

Lee, S.-S., Feingold, G., McComiskey, A., Yamaguchi, T., Koren, I., Martins, J.V., Yu, H., 2014. Effect of gradients in biomass burning aerosol on shallow cumulus convective circulations. J. Geophys. Res. Atmos. 119 (16), 9948–9964. http://dx.doi.org/10.1002/2014JD021819.

Masson, V., Gomes, L., Pigeon, G., Liousse, C., Pont, V., Lagouarde, J.-P., Voogt, J., Salmond, J., Oke, T.R., Hidalgo, J., Legain, D., Garrouste, O., Lac, C., Connan, O., Briottet, X., Lachérade, S., Tulet, P., 2008. The canopy and aerosol particles interactions in TOulouse urban layer (CAPITOUL) experiment. Meteorol. Atmos. Phys. 102 (3–4), 135–157.

Mensah, A., Holzinger, R., Otjes, R., Trimborn, A., Mentel, T.F., ten Brink, H., Henzing, B., Kiendler-Scharr, A., 2012. Aerosol chemical composition at Cabauw, The Netherlands as observed in two intensive periods in May 2008 and March 2009. Atmos. Chem. Phys. 12kk (10), 4723–4742. http://dx.doi.org/10.5194/acp-12-4723-2012.

Meszaros, R., Horvath, L., Weidinger, T., Neftel, A., Nemitz, E., Dammgen, U., Cellier, P., Loubet, B., 2009. Measurement and modelling ozone fluxes over a cut and fertilized grassland. Biogeosciences 6 (10), 1987–1999.

Morino, Y., Kondo, Y., Takegawa, N., Miyazaki, Y., Kita, K., Komazaki, Y., Fukuda, M., Miyakawa, T., Moteki, N., Worsnop, D.R., 2006. Partitioning of HNO3 and particulate nitrate over Tokyo: effect of vertical mixing. J. Geophys. Res. 111 (D15), D15,215. http://dx.doi.org/10.1029/2005JD006887.

Mozurkewich, M., 1993. The dissociation constant of ammonium nitrate and its dependence on temperature, relative humidity and particle size. Atmos. Environ. A. General Top. 27 (2), 261–270. http://dx.doi.org/10.1016/0960-1686(93)90356-4.

Nemitz, E., Sutton, M.A., 2004. Gas-particle interactions above a Dutch heathland: III. Modelling the influence of the NH3-HNO3-NH4NO3 equilibrium on size-segregated particle fluxes. Atmos. Chem. Phys. 4 (1988), 1025–1045.

Nemitz, E., Sutton, M.A., Wyers, G.P., Jongejan, P.A.C., 2004. Gas-particle interactions above a Dutch heathland: I. Surface exchange fluxes of NH_3, SO_2, HNO_3 and HCl. Atmos. Chem. Phys. 4, 989–1005.

Nenes, A., Pandis, S.N., Pilinis, C., 1998. Isorropia: a new thermodynamic equilibrium model for multiphase multicomponent inorganic aerosols. Aquat. Geochem. 4 (1), 123–152.

Noh, Y., Cheon, W., Hong, S., Raasch, S., 2003. Improvement of the k-profile model for the planetary boundary layer based on large eddy simulation data. Boundary-Layer Meteorol. 107 (2), 401–427. http://dx.doi.org/10.1023/A:1022146015946.

Saleh, R., Donahue, N.M., Robinson, A.L., 2013. Time scales for gas-particle partitioning equilibration of secondary organic aerosol formed from alpha-pinene ozonolysis. Environ. Sci. Technol. 47 (11), 5588–5594. http://dx.doi.org/10.1021/es400078d.

Shiraiwa, M., Seinfeld, J.H., 2012. Equilibration timescale of atmospheric secondary organic aerosol partitioning. Geophys. Res. Lett. 39 (24) http://dx.doi.org/10.1029/2012GL054008.

Slinn, S.A., Slinn, W., 1980. Predictions for particle deposition on natural waters. Atmos. Environ. 14, 1013–1016.

ten Brink, H., Otjes, R., Jongejan, P., Slanina, S., 2007. An instrument for semi-continuous monitoring of the size-distribution of nitrate, ammonium, sulphate and chloride in aerosol. Atmos. Environ. 41 (13), 2768–2779. http://dx.doi.org/10.1016/j.atmosenv.2006.11.041.

Thomas, R.M., Trebs, I., Otjes, R., Jongejan, P.A.C., Ten Brink, H., Phillips, G., Kortner, M., Meixner, F.X., Nemitz, E., 2009. An automated analyzer to measure surface-atmosphere exchange fluxes of water soluble inorganic aerosol compounds and reactive trace gases. Environ. Sci. Technol. 43 (5), 1412–1418.

Troen, I., Mahrt, L., 1986. A simple model of the atmospheric boundary layer; sensitivity to surface evaporation. Boundary-Layer Meteorol. 37 (1–2), 129–148.

van Heerwaarden, C.C., Vilà-Guerau de Arellano, J., Gounou, A., Guichard, F., Couvreux, F., 2010. Understanding the daily cycle of evapotranspiration: a method to quantify the influence of forcings and feedbacks. J. Hydrometeorol. 11 (6), 1405–1422. http://dx.doi.org/10.1175/2010JHM1272.1.

Velders, G.J.M., Geilenkirchen, G.P., Lange, R.D., 2011. Higher than expected NOx

emission from trucks may affect attainability of NO2 limit values in the Netherlands. Atmos. Environ. 45 (18), 3025–3033. http://dx.doi.org/10.1016/j.atmosenv.2011.03.023.

Velthof, G.L., Bruggen, C.V., Groenestein, C.M., Haan, B.J.D., Hoogeveen, M.W., Huijsmans, J.F.M., 2012. A model for inventory of ammonia emissions from agriculture in the Netherlands. Atmos. Environ. 46, 248–255. http://dx.doi.org/10.1016/j.atmosenv.2011.09.075.

Vermeulen, A.T., Hensen, A., Popa, M.E., van den Bulk, W.C.M., Jongejan, P.A.C., 2011. Greenhouse gas observations from cabauw tall tower (19922010). Atmos. Meas. Tech. 4 (3), 617–644. http://dx.doi.org/10.5194/amt-4-617-2011.

Verver, G., 1994. Comment on "A modified K model for chemically reactive species in the planetary boundary laye" by Fujihiro Hamba. J. Geophys. Res. 99 (94), 21–23.

Vilà-Guerau de Arellano, J., Duynkerke, P., 1992. Influence of chemistry on the flux gradient relationships for the NO-O3-NO2 system. Boundary-Layer Meteorol. 61, 375–387.

Vilà-Guerau de Arellano, J., Duynkerke, P.G., 1995. Atmospheric surface layer similarity theory applied to chemically reactive species. J. Geophys. Res. 100, 1397–1408. http://dx.doi.org/10.1029/94JD02434.

Vilà-Guerau de Arellano, J., Kim, S.-W., Barth, M.C., Patton, E.G., 2005. Transport and chemical transformations influenced by shallow cumulus over land. Atmos. Chem. Phys. 5, 3219–3231. http://dx.doi.org/10.5194/acp-5-3219-2005.

Vilà-Guerau de Arellano, J., Patton, E.G., Karl, T., van den Dries, K., Barth, M.C., Orlando, J.J., 2011. The role of boundary layer dynamics on the diurnal evolution of isoprene and the hydroxyl radical over tropical forests. J. Geophys. Res. Atmos. 116 (D7) http://dx.doi.org/10.1029/2010JD014857.

Vinuesa, J.-F., Vilà-Guerau de Arellano, J., 2003. Fluxes and (co-)variances of reacting scalars in the convective boundary layer. Tellus B 55 (4), 935–949. http://dx.doi.org/10.1046/j.1435-6935.2003.00073.x.

Wang, P., Knap, W.H., Kuipers Munneke, P., Stammes, P., 2009. Clear-sky shortwave radiative closure for the Cabauw baseline surface radiation network site, Netherlands. J. Geophys Res. 114 (D14), D14,206. http://dx.doi.org/10.1029/2009JD011978.

Wolff, V., Trebs, I., Foken, T., Meixner, F.X., 2010. Exchange of reactive nitrogen compounds : concentrations and fluxes of total ammonium and total nitrate above a spruce canopy. Biogeosciences 7, 1729–1744. http://dx.doi.org/10.5194/bg-7-1729-2010.